Spectral Observation Theory and Beam Debroadening Algorithm for Atmospheric Radar

Koji Nishimura[ID], Masashi Kohma, Kaoru Sato, and Toru Sato

Abstract—In order to measure the variance of wind velocity, which is contributed from turbulence, via radar observations, it is necessary to remove the unwanted contribution from strong horizontal velocity components through the finite beamwidth of the radar. This effect is referred to as beam broadening. Although the amount of beam broadening has thus far been calculated based on the approximating assumption that the pattern of the beam is rotationally symmetric and has very low sidelobes, we need to take a more theoretical approach to radar—one that does not have a simple beam pattern like the Antarctic Program of the Antarctic Syowa Station (PANSY) radar (69S, 39E). In this article, we clarify the theoretical relationship in a very simple form between the turbulence spectrum, which is directly associated with the variance of turbulence, two-way beam patterns, and the observed spectrum, using autocorrelation functions (ACFs). The theory is thoroughly universal and applicable to any type of atmospheric radar, such that we can quantitatively analyze radar observation systems. Furthermore, we propose a "debroadening" algorithm based directly on this theory and from calculations of the general maximum likelihood (ML). We performed numerical simulations that validate our theory and the algorithm.

Index Terms—Atmospheric radar, mesosphere-stratosphere-troposphere (MST) radar, beam broadening, debroadening, turbulence.

I. INTRODUCTION

MEASURING the variance of the velocity of the atmosphere σ_{turb}^2, which is proportionally linked to the energy dissipation rate, is a common role given to mesosphere-stratosphere–troposphere (MST) radar. However, the spectral width σ_{obs}, which is observable directly with radar, contains not only the contribution from turbulence itself (σ_{turb}^2) but also some measurement biases due to the vertical variation of the velocity (σ_{shear}^2), the temporal variation of the velocity (σ_{time}^2), and projection components of the mean wind velocity to the off-center sensitivity of the radar beam (σ_{beam}^2) [1]. Here, σ_{shear}^2,

Koji Nishimura is with the Research Organization of Information and Systems, Tokyo 105-0001, Japan, and also with the National Institute of Polar Research, Tachikawa 1908518, Japan (e-mail: knish@nipr.ac.jp).

Masashi Kohma and Kaoru Sato are with the Department of Earth and Planetary Science, The University of Tokyo, Tokyo 1130033, Japan.

Toru Sato is with the Department of Communications and Computer Engineering, Kyoto University, Kyoto 6068501, Japan.

σ_{time}^2, and σ_{beam}^2 are commonly referred to as shear, time, and beam broadening, respectively. Therefore, in a symbolic sense, the observed spectral width σ_{obs} is expressed as

$$\sigma_{\text{obs}}^2 = \sigma_{\text{turb}}^2 + \sigma_{\text{beam}}^2 + \sigma_{\text{shear}}^2 + \sigma_{\text{time}}^2 + \text{error}. \quad (1)$$

These unwanted components often become much larger than σ_{turb}^2 itself, and as such cannot be ignored.

Among these components, σ_{shear}^2 and σ_{time}^2 are induced by the variance of wind velocity in height and time, respectively. Typically, these components are estimated by tracing the variation of the mean Doppler shift (spectral mean) along height and time, respectively, and then removed.

The remaining broadening component, σ_{beam}^2, is caused by the finite radar beamwidth, typically up to a few degrees. This results in variability of the projection angle to the mean wind velocity vector, giving different Doppler shifts with respect to the mean wind velocity from one part to another in the beam. With respect to this effect, a series of comprehensive studies has been conducted by Hocking [2]–[4]. They assumed that the radar beam is rotationally symmetric and that the beam pattern (e.g., the polar gain diagram) is characterized simply by the beamwidth θ_{beam} with no sidelobes. Recently, the impact of neglecting the sidelobes in estimating the strength of the turbulence is evaluated by Sommer and Chau [5]. They concluded therein that even the standard sidelobe level (~ -18 dB) for circular aperture should be taken into account for evaluating turbulence.

Via considerations on the simplified radar beam model, it has been a common understanding that the beam broadening should be expressed as a convolution of "beam broadening" spectrum the width of which is proportional to the mean background wind velocity and the "true" turbulent spectrum in the frequency domain. Accordingly, it has also been known that this can be expressed more simply in the "correlation domain" as a multiplication of the two autocorrelation functions corresponding to the "beam broadening" and "true" spectra [6]–[9].

Following these studies, VanZandt *et al.* [10] proposed a variational technique to estimate σ_{turb}^2 by taking advantage of two different beam widths. However, this technique is also based on the assumption that the main beam is almost rotationally symmetric and well defined by its width, and that the sidelobes are negligible.

Although most of the existing MST and wind profiler radars have a uniform antenna array with approximately circular or rectangular arrangements, those with a distributed and asymmetric array complicate the evaluation of the

turbulence spectrum. The Program of the Antarctic Syowa Station (PANSY) MST/IS Radar (69.0°S, 39.6°E) is one such example. PANSY radar is the first MST/IS radar installed in the Antarctic. It has a large phased array consisting of 1045 antennas [11]. This radar has a distributed and asymmetric antenna arrangement, and consequently a complicated beam pattern.

This is because we needed to rearrange and spread the arrangement to avoid heavy snow accumulation due to its density, after the one we experienced in 2012. The resulting antenna arrangement and its beam patterns are shown later. For this reason, we cannot apply simplifications as in the earlier studies. Alternatively, a versatile and thorough mathematical approach is needed so as not to exclude any radar design.

In what follows, we develop a mathematical theory that describes how the power spectrum of the radar echoes is formed with respect to the two-way complex-valued beam pattern and the velocity spectrum of the atmospheric turbulence. We further propose a debroadening algorithm that is formed simply using this relationship, namely an inverse calculation that obtains the true turbulence spectrum given the series of radar echoes or a power spectrum.

This article is organized as follows. In Section II, we develop the mathematical formulation of the radar observation to derive an expression of the observation function, or, in other words, the two-way beam pattern. Section III is the core part of this article in which we develop the mathematical theory of the radar echo, the turbulence spectrum, and the observation function (beam pattern). In this section, it is proven that the autocorrelation of the received echo is merely a multiplication of the autocorrelations of the turbulence and the observation function. In Section IV, we propose a numerical debroadening algorithm that estimates the true turbulence spectrum by removing the effect of the beam pattern. In Section V, we describe numerical simulations that demonstrate that our theory and algorithm works as we expect. In Section VI, we place some discussion about the impact on scientific analyses, and also technical implementations. In Section VII, we state some concluding remarks. Note that we separate some mathematical descriptions in Appendixes A and B in order to keep the structure of this article as simple as possible.

In the following discussion, the words "power spectrum" and "autocorrelation" often appear. As is well known, the two of them are the Fourier transform to each other and have very similar information. Although we choose a word of the two that fits more in the context, one would want to replace it by the other when it is confusing.

II. RADAR OBSERVATION FUNCTION

We first formulate the radar observation system as a function of space. A basic formulation is detailed, for example, in Hocking *et al.* [12]. We consider that the target atmosphere is three-dimensionally gridded in cubic cells as schematically depicted in Fig. 1, with dimensions $L_1 \times L_2 \times L_3$, where $L_{[\cdot]}$ can be $L_{[\cdot]} \gg \lambda/2$ to reduce the computational cost. In order to avoid complexities in description, we use the single dimension
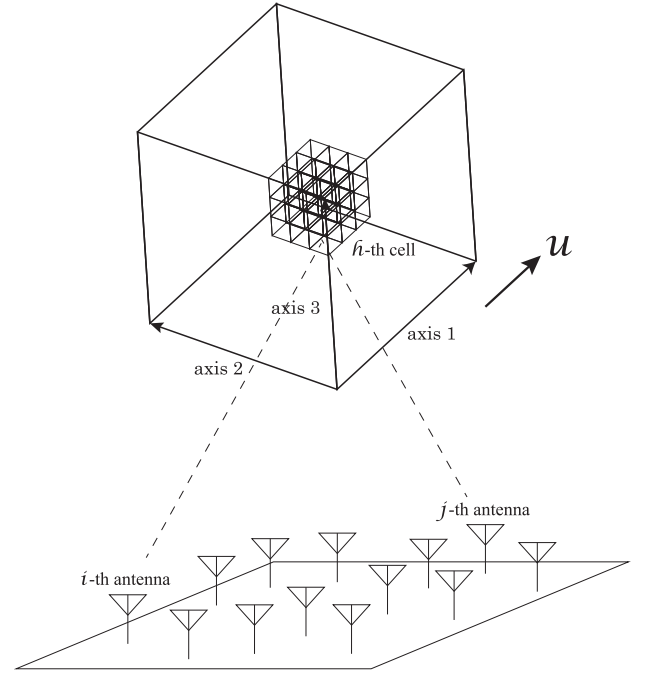

Fig. 1. Grid configuration: the cells are arranged such that the first axis matches the direction of the wind vector.

factor L that is $L_1 = L_2 = L_3 = L$ throughout this article. This is not an essential restriction in the following theory.

The arrangement of the grid is as follows. We set the first axis of the grid parallel to the mean wind vector $\boldsymbol{u}$. We do not consider the case in which $\boldsymbol{u}$ is completely vertical or 0. The second axis is set horizontally and perpendicular to $\boldsymbol{u}$. Finally, the third axis is set perpendicular to the first two axes.

Let k, l, and m be integer indices of the position of cells along the first, second, and third axes, respectively. The positions of cells $\boldsymbol{x}_{klm}, \boldsymbol{x}_{(k+1)lm}, \boldsymbol{x}_{(k+2)lm}, \ldots$ are consequently aligned along the mean wind direction. In order to avoid the complexity of subscripts, when exact 3-D positions are unnecessary, we use an alternative serial index h like $\boldsymbol{x}_h$ instead of k, l, and m. Thus, the following operators are equivalent:

$$\sum_h = \sum_k \sum_l \sum_m = \sum_{klm}. \qquad (2)$$

Let $\boldsymbol{x}_i$ and $\boldsymbol{x}_j$ denote the positions of the ith and jth antennas, respectively, and let $\boldsymbol{x}_h(t)$ be the position of the hth target cell at time t. Time t is divided into two parts: $t = t_n + T$, where slow time $t_n = nt_\Delta$ is the time point of the nth pulse transmission where t_Δ is the interval; and fast time T; $0 < T < t_\Delta$, the lapse time after the pulse transmission at t_n.

We first consider a path of the signal transmitted from antenna i, scattered by target cell h, and then received by antenna j. Let $p_i(t)$ be the transmitted signal, $f_h(t)$ the scattering coefficient at cell h as a function of time, and $q_j(t)$ the receiver filter. Standardly, $q_j(t)$ contains a matched filter and a frequency conversion, and then the signal is sampled at the fast time T in accordance with the nominal range $R = cT/2$, where c is the speed of light. The sampled signal

corresponding to a nominal range R thus becomes

$$r_{hij}(t_n) = \int_0^{t_\Delta} f_h\left(t_n + T - \frac{|\boldsymbol{x}_h - \boldsymbol{x}_i|}{c}\right)$$
$$\times p_i\left(T - \frac{|\boldsymbol{x}_h(t_n) - \boldsymbol{x}_i| + |\boldsymbol{x}_h(t_n) - \boldsymbol{x}_j|}{c}\right)$$
$$\times q_j\left(T - \frac{2R}{c}\right) dT. \tag{3}$$

The scattering coefficient function $f_h(t)$ varies in time depending on the state of the atmosphere, and it can be treated as constant during one pulse repetition interval t_Δ; therefore, $f_h(t_n + T) \simeq f_h(t_n)$, $T \leq t_\Delta$.

Then

$$r_{hij}(t_n) = f_h(t_n) \int_0^{t_\Delta} p_i\left(T - T_{hij}(t_n)\right) q_j(T - T_R) dT \tag{4}$$

where $T_{hij}(t_n)$ denotes the time of flight between antennas i and j via target cell h as a function of slow time t_n. That is

$$T_{hij}(t_n) = \frac{|\boldsymbol{x}_h(t_n) - \boldsymbol{x}_i| + |\boldsymbol{x}_h(t_n) - \boldsymbol{x}_j|}{c} \tag{5}$$

and

$$T_R = \frac{2R}{c} \tag{6}$$

is the sampling time corresponding to the nominal range.

The integration in (4), a cross correlation of $p_i(t)$ and $q_j(t)$, consists only of known functions and can be calculated apart from the received signal. When we define

$$g'_{ij}(\tau) = \int_0^{t_\Delta} p_i(T) q_j(T - T_R + \tau) dT \tag{7}$$

we can rewrite (4) as

$$r_{hij}(t_n) = f_h(t_n) g'_{ij}\left(T_{hij}(t_n)\right). \tag{8}$$

For simplicity, we define $g_{hij}(t_n) = g'_{ij}(T_{hij}(t_n))$, and (8) becomes

$$r_{hij}(t_n) = f_h(t_n) g_{hij}(t_n). \tag{9}$$

In the case of monostatic radar with antennas indexed with $i = 1, 2, \ldots, N_{\text{ant}}$, a combined receiver signal in terms of target cell h is

$$r_h(t_n) = f_h(t_n) \sum_i^{N_{\text{ant}}} \sum_j^{N_{\text{ant}}} g_{hij}(t_n)$$
$$= f_h(t_n) g_h(t_n) \tag{10}$$

where $g_h(t_n)$ is the sum of $g_{hij}(t_n)$ through i and j. Again, in (10), $f_h(t_n)$ is the scattering coefficient (usually real-valued) of target cell h, and $g_h(t_n)$ is the complex beam pattern (i.e., the receiver filter form considered) with respect to the target cell's position $\boldsymbol{x}_h(t_n)$.

III. DERIVATION OF AUTOCORRELATION FUNCTION (ACF) AND POWER SPECTRUM

In the previous section, we derived a form of the received signal as a function of the scattering coefficient at gridded cells of the target atmosphere. We now turn to the derivation of a form of the power spectrum of the echo from the received signal. Unlike most radar systems, we exploit the ACF with which the final result is given in a simpler form than the one with the power spectrum. Furthermore, in this section, we treat slow time t_n as continuous t for the sake of simplicity, insofar as doing so does not significantly alter our conclusions.

Signals received at the antennas are added to a single series of signal $r(t)$. That is

$$r(t) = \sum_h f_h(t) g_h(t). \tag{11}$$

In order to derive the autocorrelation of the signal, we place two assumptions or approximations of the scattering coefficient functions of the gridded atmosphere cells.

1) *Independence:* $f_h(t) \perp\!\!\!\perp f_{h'}(t)$ for $h \neq h'$.
2) *Spectral equality:* $\mathrm{E}|\mathscr{F}_t[f_h(t)]|^2 = \mathrm{E}|\mathscr{F}_t[f_{h'}(t)]|^2$.

where the operators $\perp\!\!\!\perp$, E, and $\mathscr{F}_t$ denote independence, the ensemble expectation, and the Fourier transform with respect to time t, respectively. Assumptions 1 and 2 mean that the scattering coefficient functions are independent at one cell to another as a time series with the same power spectrum. As a corollary of Assumption 2, with respect to the ACFs, the equality $F_h(\tau) = F_{h'}(\tau) = F(\tau)$ is also true for any h and h', where $F_h(\tau)$ is the ACF of $f_h(t)$. The unsubscripted $F(\tau)$ is the common expression for all cells.

The ACF of the received signal $r(t)$ is mathematically defined by an integration of a signal of infinite time

$$R_\infty(\tau) = \int r^*(t) r(t + \tau) dt \tag{12}$$

where $*$ operator denotes complex conjugation. Obviously, we need to consider finite time observations in practice. From the mathematical point of view, however, an autocorrelation with a finite time integration is subject to statistical fluctuations. To bridge the gap between the theoretical autocorrelation and the practical observations, we first consider an ensemble of an infinite number of segmented time observations in order to obtain a mathematical expression of autocorrelation that statistically converges.

Let $r_\zeta(t)$ be the observed signal with respect to the integer index of the ensemble experiment ζ. Then, an ensemble averaged ACF is

$$R(\tau) = \mathrm{E} \int \left\{r_\zeta(t) w(t)\right\}^* \left\{r_\zeta(t + \tau) w(t + \tau)\right\} dt \tag{13}$$

where $w(t)$ is a rectangular window function for taking into account the time duration D. That is, as also shown in Fig. 2

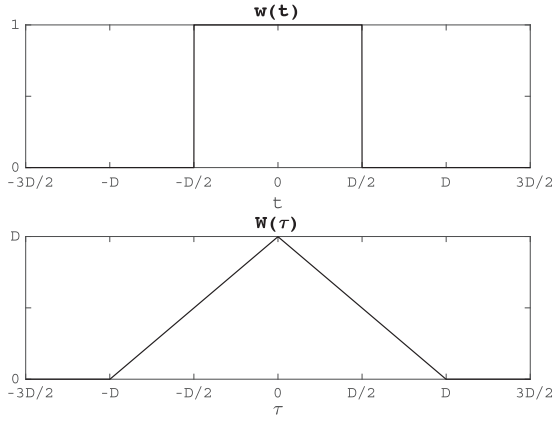$$w(t) = \begin{cases} 1, & -D/2 < t \leq D/2 \\ 0, & \text{otherwise.} \end{cases} \tag{14}$$

Fig. 2.   Rectangular window function $w(t)$ and its ACF $W(\tau)$ are plotted.
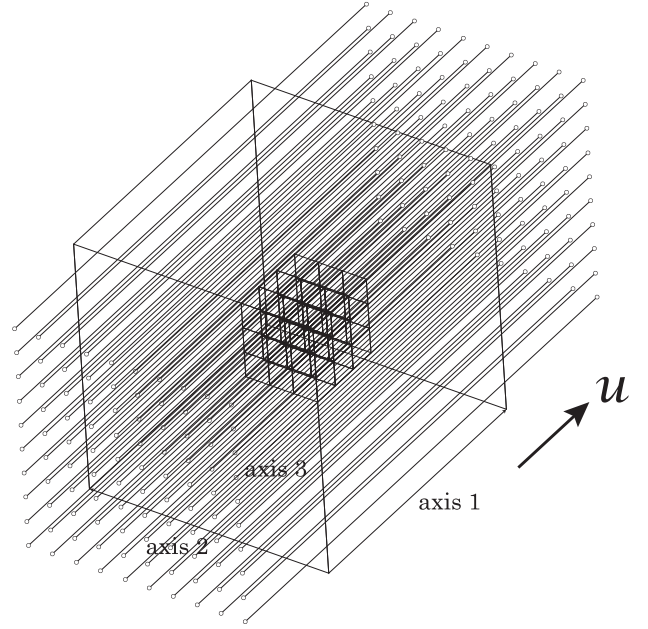

Fig. 3.   Schematic illustration of the cells. In order to derive the function $F(\tau)$, every string of cells along Axis 1 is regarded as a discrete time series with increments at every $L/|u|$.

Substituting (11) in (13), we obtain

$$
R(\tau) = \mathrm{E} \int \left\{ \sum_h f_{h\zeta}^*(t)\, g_h^*(t)\, w^*(t) \right\}
$$

$$
\times \left\{ \sum_{h'} f_{h'\zeta}(t+\tau)\, g_{h'}(t+\tau)\, w(t+\tau) \right\} \mathrm{d}t \quad (15)
$$

$$
= \mathrm{E} \int \sum_h \sum_{h'} f_{h\zeta}^*(t)\, f_{h'\zeta}(t+\tau)
$$

$$
\times \; g_h^*(t)\, g_{h'}(t+\tau)\, w^*(t)\, w(t+\tau)\, \mathrm{d}t \quad (16)
$$

$$
= \int \sum_h \sum_{h'} \mathrm{E}\big[f_{h\zeta}^*(t)\, f_{h'\zeta}(t+\tau) \big]
$$

$$
\times \; g_h^*(t)\, g_{h'}(t+\tau)\, w^*(t)\, w(t+\tau)\, \mathrm{d}t. \quad (17)
$$

In (17), the expectation operator is applied only to the bracket that contains $f_{h\zeta}^*(t)\, f_{h'\zeta}(t+\tau)$ because this part is the only stochastic signal, whereas the other parts are deterministic. When $h \neq h'$, $\mathrm{E}[f_{h\zeta}^*(t)\, f_{h'\zeta}(t+\tau)] = 0$ because $f_{h\zeta}^*(t) \perp\!\!\!\perp f_{h'\zeta}(t+\tau)$ for any $h \neq h'$ according to Assumption 1. Then, $\mathrm{E}[\, f_{h\zeta}^*(t)\, f_{h\zeta}(t+\tau)\,]$ (i.e., the case of $h = h'$) should be independent of t, because of stationarity, and from h, because of Assumption 2. Accepting the ergodic hypothesis, we can replace the expectation with a temporal integration: we thus obtain

$$
\mathrm{E}\big[f_{h\zeta}^*(t)\, f_{h\zeta}(t+\tau) \big] = \int f_{h\zeta}^*(t)\, f_{h\zeta}(t+\tau)\, \mathrm{d}t \quad (18)
$$

$$
= F(\tau) \quad (19)
$$

where $F(\tau)$ is the unique ACF common to all the cell indices h and experiment indices ζ. Thus

$$
\mathrm{E}\big[f_{h\zeta}^*(t)\, f_{h'\zeta}(t+\tau) \big] = \begin{cases} F(\tau), & h = h' \\ 0, & h \neq h'. \end{cases} \quad (20)
$$

Substituting (20) in (17), we obtain

$$
R(\tau) = \int \sum_h F(\tau)\, g_h^*(t)\, g_h(t+\tau)\, w^*(t)\, w(t+\tau)\, \mathrm{d}t \quad (21)
$$

$$
= F(\tau) \int \sum_h \big[g_h^*(t)\, g_h(t+\tau) \big]\, w^*(t)\, w(t+\tau)\, \mathrm{d}t. \quad (22)
$$

In (22), the summation operator is applied only to $g_h^*(t)\, g_h(t+\tau)$ because this is the only term dependent on h that remains in the integrand. We now expand the serial index h to a set of 3-D indices k, l, and m, as explained in Section II. Then, the summation becomes

$$
\sum_h g_h^*(t)\, g_h(t+\tau) \quad (23)
$$

$$
= \sum_m \sum_l \sum_k g_{klm}^*(t)\, g_{klm}(t+\tau) \quad (24)
$$

$$
= \sum_m \sum_l \left[\sum_k g_{lm}^*\left(t + \frac{kL}{|u|} \right) g_{lm}\left(t + \frac{kL}{|u|} + \tau \right) \right] \quad (25)
$$

where $g_{lm}^*(t + kt_\Delta)$ is a 1-D section of the complex beam function along the mean wind direction u shown in Fig. 3, sampled at time interval $kL/|u|$ corresponding to grid interval L.

When we look at the summation in terms of k in (25), $\sum_k g_{lm}^*(t + kL/|u|)\, g_{lm}(t + kL/|u| + \tau)$, it takes the form of an ACF having a summation with respect to k instead of in integration by t. Assuming $g_{lm}^*(t)$ are smooth functions and the sampling interval $kL/|u|$ corresponding to the spatial interval L is sufficiently dense, we define

$$
G_{lm}(\tau) = \sum_k g_{lm}^*\left(t + \frac{kL}{|u|} \right) g_{lm}\left(t + \frac{kL}{|u|} + \tau \right) \quad (26)
$$

where $G_{lm}(\tau)$ is the ACF of $g_{lm}(t)$.

We now define $G(\tau)$ as the sum of all ACFs $G_{lm}(\tau)$ of the complex beam functions $g_{lm}(t)$ indexed with l and m, which is

$$
G(\tau) = \sum_m \sum_l G_{lm}(\tau) = \sum_h g_h^*(t)\, g_h(t+\tau). \quad (27)
$$

In function $G(\tau)$, time lag τ has a relationship to the spatial distance along the x-axis via the velocity of the wind u.

Specifically, $\tau = \xi/|\boldsymbol{u}|$ where ξ is the spatial lag along the x-axis, and thus

$$G(\tau) = G(\xi/|\boldsymbol{u}|). \qquad (28)$$

Substituting (27) into (22), we obtain

$$R(\tau) = F(\tau) \int G(\tau)\, w^*(t)\, w(t+\tau)\, \mathrm{d}t \qquad (29)$$

$$= F(\tau)\, G(\tau) \int w^*(t)\, w(t+\tau)\, \mathrm{d}t. \qquad (30)$$

The remaining integration is simply the ACF of the window function. Therefore, (30) can be rewritten as

$$R(\tau) = F(\tau)\, G(\tau)\, W(\tau). \qquad (31)$$

The final form of $R(\tau)$ in (31) states a remarkable relationship between the four ACFs. Note that the result is not trivial, because, in general, $R_{dd}(\tau) = R_{aa}(\tau) R_{bb}(\tau) R_{cc}(\tau)$ does not hold where $R_{dd}(\tau)$ is the ACF of $d(t) = a(t)\, b(t)\, c(t)$, and the other $R_{..}(\tau)$ are similarly defined, given that $a(t)$, $b(t)$, and $c(t)$ are arbitrary functions.

IV. ALGORITHM TO ESTIMATE $F(\tau)$

In this section, we derive a practical algorithm to estimate the spectrum of $f(t)$ from the observed spectrum of $r(t)$, based on the relationship described in (31). In order to develop the numerical algorithms, we employ the following discrete expressions:

$$r[n] = \sum_h f_h[n]\, g_h[n] \qquad (32)$$

and

$$R[\nu] = F[\nu]\, G[\nu]\, W[\nu] \qquad (33)$$

instead of

$$r(t) = \sum_h f_h(t)\, g_h(t) \qquad (34)$$

and

$$R(\tau) = F(\tau)\, G(\tau)\, W(\tau) \qquad (35)$$

where n denotes the integer index of slow time $t_n = n\, t_\Delta$, and ν denotes the integer index of the time lags τ.

In addition, we assume that the observed spectrum is given in the form of an averaged periodogram (also known as the Bartlett method) that is defined by the sum of the absolute square of the discrete Fourier transform (DFT) of the received signals. That is

$$\mathcal{R}[\kappa] = \sum_{\zeta=0}^{N_{\text{ens}}-1} \left| \sum_{n=0}^{N_{\text{dft}}-1} r\left[n_\zeta + n\right] \exp\left(j 2\pi\kappa \frac{n}{N_{\text{dft}}}\right) \right|^2 \qquad (36)$$

where κ is the integer index for the discrete frequency, N_{dft} is the length of the signal segment for the DFT, and N_{ens} is the number of ensemble averaging, or incoherent averaging. The offset index n_ζ is selected such that the signal segments do not overlap in different DFT segments with the Bartlett method. That is

$$n_\zeta = \zeta\, N_{\text{dft}}. \qquad (37)$$

We now want to solve (33) with respect to $F[\nu]$ given $R[\nu]$, $G[\nu]$ and $W[\nu]$. One simple way to do so is to calculate $R[\nu]/(G[\nu]W[\nu])$, but this solution is too sensitive to noise contained in $R[\nu]$ and does not usually provide a satisfactory result. Instead, we apply a simple parametric inversion method.

The most widely accepted parametric spectrum model for atmospheric echo is the four-parameter Gaussian model (e.g., [13], see also Appendix B). Accepting a Gaussian spectral model, we are able to apply a Gaussian temporal autocorrelation model as well. The four-parameter Gaussian autocorrelation model is defined as

$$F[\nu] = A\frac{\sqrt{2\pi}\,\sigma}{N}\exp\left[-\frac{2\pi^2\sigma^2\nu^2}{N^2}+j\frac{2\pi\nu\mu}{N}\right]+P_n\,\delta[\nu] \quad (38)$$

where A, σ, μ, and P_n are the amplitude, spectral width, spectral mean, and noise level, respectively. $\delta[\nu]$ is the discrete delta function, which is $\delta[0]=1$ and $\delta[\nu]=0 \ \forall\ \nu\neq 0$.

Once we obtain $G[\nu]$, given a wind velocity vector $\boldsymbol{u}$, we can calculate a theoretical $R[\nu]$ according to (33). By applying the DFT to $R[\nu]$ following (41) in Appendix A, we obtain a theoretical spectrum curve $\mathcal{R}[\kappa]$. Let $\mathcal{R}_{\text{obs}}[\kappa]$ be a spectrum calculated by (41) or (46) from observed data. By comparing $\mathcal{R}[\kappa]$ and $\mathcal{R}_{\text{obs}}[\kappa]$, we can evaluate how close the theoretical spectrum is to the one observed. One of the most popular ways of evaluating the goodness of fit of $\mathcal{R}[\kappa]$ is the least mean squared (LMS) method in which the squared sum of the residue between the two is evaluated.

Another evaluation method is the maximum likelihood (ML), which pursues the maximization of the likelihood as a function $\mathcal{R}[\kappa]$ with respect to $\mathcal{R}_{\text{obs}}[\kappa]$, considering every $\mathcal{R}[\kappa]$ at an integer κ as a scalar random variable that follows a class of gamma distribution, which a sum of squares of Gaussian random variables obey (often mentioned as "χ^2 distribution" in a not so rigorous situation). The ML technique is detailed, for example, by Rice [14]. In this article, we employ the ML method to demonstrate our proposed technique.

An example of an algorithm that estimates the optimal parameters $\hat{A}$, $\hat{\sigma}_v$, $\hat{\mu}$, and $\hat{P}_n$, and the corresponding spectrum $\mathcal{R}[\kappa]$, given $\mathcal{R}_{\text{obs}}[\kappa]$, is summarized as follows.

Algorithm:
1) Initialize A, σ_v, μ, and P_n;
2) Calculate the initial $\mathcal{R}[\kappa]$;
3) Calculate the initial likelihood;
4) Modify A, σ_v, μ, and P_n;
5) Calculate $\mathcal{R}[\kappa]$;
6) Calculate the likelihood;
7) Return to Step 4 unless the likelihood reaches the maximum.

Since analytic expressions of the derivatives of the likelihood are difficult to obtain, optimization methods that do not require the gradient vector should be applied.

V. NUMERICAL SIMULATIONS

A. General Characteristics

In order to validate and evaluate the algorithm we derived in the previous sections, we conducted simple numerical simulations. Our simulation was based on the PANSY radar
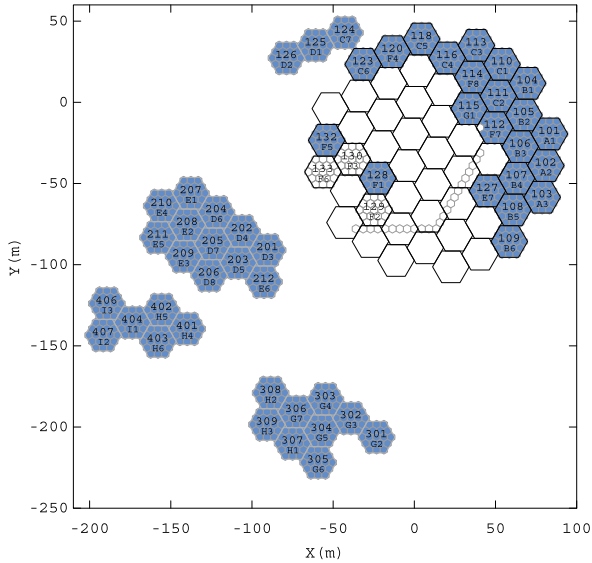
Fig. 4. Antenna array of PANSY radar, in January 2017. The small hexagons filled in blue show the positions of the antennas, where the larger hexagons circumscribing 19 of them each indicate independent subarrays.

hardware with an operational frequency $f_0 = 47$ MHz. The antenna arrangement is shown in Fig. 4.

The forward calculation model of the simulations to obtain $\mathcal{R}_{\mathrm{obs}}[\kappa]$ was based on the grid model shown in Fig. 1. Therein, the grid size was set to $L = 30$ m. Mean wind velocity was set to $|\boldsymbol{u}| = 46.0$ ms^{-1}, with six different azimuth angles $0, 60, \ldots$, and 300. The beam direction was set to the zenith. The envelope of the transmitted pulse was shaped to the Gaussian with the full-width at half-maximum (FWHM) of $1 \mu s$. Consequently, the range resolution was 150 m. The nominal range (height) was $R = 6000$ m.

Fig. 5 shows 2-D (horizontal) and 1-D sections of complex beam patterns in Rows (a) and (b), $G(\tau)$ in Row (c), and its Fourier transform in Row (d). Therein, Row (a) shows the horizontal section of the complex beam pattern at a height of 6000 m rotated by the angle designated to each column such that the x-axis agrees with the direction of $\boldsymbol{u}$. The pairs of Columns 1 and 4, 2 and 5, and 3 and 6 have opposite wind direction. The x-sections of the beam and their RMS envelopes are exhibited in Row (b). These plots are clipped within the range $x \in [-400, 400]$ m for visual presentation; the calculations were done at a wider range. Row (c) shows the complex ACFs $G'(\xi)$ as a function of spatial lag ξ instead of $G(\tau)$. They are related as $G'(\xi) = G(\xi/|\boldsymbol{u}|) = G(\tau)$. One notable characteristic the ACFs show is that echoes lose their correlation when the target moves by ~ 200 m, regardless of how the original beam pattern spreads in space. Another characteristic is that the ACFs have some phase rotation even when the wind is horizontal while the beam is vertical. This is due to the asymmetric arrangement of the array.

Row (d) shows the Fourier transforms of the ACFs $G(\tau)$ plotted in Row (c) as functions of frequency in arbitrary units (or 1/distance) to illustrate their difference in shape. We refer to this function as the broadening spectrum. The pairs with opposite wind direction show the symmetric appearance

Model Parameter	Symbol	Value	Unit
Frequency	f_0	47.0	MHz
Half wavelength	$c/2f_0$	3.189	m
Wind velocity	$|\boldsymbol{u}|$	46.0	ms^{-1}
Sampling interval (in time)	t_Δ	128	ms
No. of samples in one DFT	N_{dft}	128	
Length of one DFT segment	$t_\Delta N_{\mathrm{dft}}$	16.384	s
No. of incoherent integrations	N_{ens}	7	
Interval in frequency	$f_\Delta = 1/t_\Delta N_{\mathrm{dft}}$	0.061	Hz
Interval in velocity	$c/2f_0 t_\Delta N_{\mathrm{dft}}$	0.195	ms^{-1}
Spectral amplitude	A	10.0	
Spectral mean	μ	0.0	
Spectral width	σ	1.0	
Spectral noise floor	P_n	1.0	

with respect to zero in frequency corresponding to the phase rotation in their ACFs. This means that the final Doppler spectra have different frequency offsets depending on the wind direction, even if the beam is vertical to the horizontal wind.

B. Estimating Doppler Spectra

The parameters to simulate "observed" spectra $\mathcal{R}_{\mathrm{obs}}[\kappa]$ are summarized in Table I. Employing the estimation algorithm derived, we simulated $\mathcal{R}_{\mathrm{obs}}[\kappa]$ given the Gaussian spectral parameters $A = 10$, $\mu = 0$, $\sigma = 1$, and $P_n = 1$. μ and σ are normalized by the frequency interval and dimensionless, such that $\sigma = 1$ corresponds to f_Δ in Hz. In the following part, errors of the estimates with respect to μ and σ are also given dimensionless unless units are accompanied explicitly.

In order to demonstrate the performance of our proposed algorithm, we employed the LMS method without the debroadening algorithm as a conventional technique for comparison. The resulting estimates via our proposed and the conventional algorithms are shown in Fig. 6. With respect to mean Doppler shift μ [see Fig. 6(a)], the estimates via our proposed algorithm (blue) shows a very good agreement with the given truth ($\mu = 0.0$) with a maximum absolute error of 0.02 (~ 4 mm/s), whereas the result from the conventional technique (red) gives 0.25 (~ 49 mm/s). With respect to spectral width σ [see Fig. 6(b)], our proposed algorithm (blue) shows a very good agreement with the given truth ($\mu = 0.0$) with maximum absolute error of 0.05 (~ 9 mm/s), whereas the result from the conventional technique (red) gives 0.80 (~ 157 mm/s).

Note that with the conventional technique an estimate of μ is biased as if the beam is tilted, whereas actually the array is uniformly excited. This is because an asymmetric antenna array has a deformed beam pattern in the near field having the main spot of the beam off-centered. We would like to refer to this effect as the *pseudo tilt effect*. In the example we demonstrate above, the pseudo tilt angle corresponds approximately to 0.06°. Since this effect disappears in the far-field at the infinite range, it is not really reasonable to compensate for the pseudo tilting using physical beam steering. Our proposed method does not have the pseudo tilt issue because it solves the inverse problem, which automatically takes this effect into account.
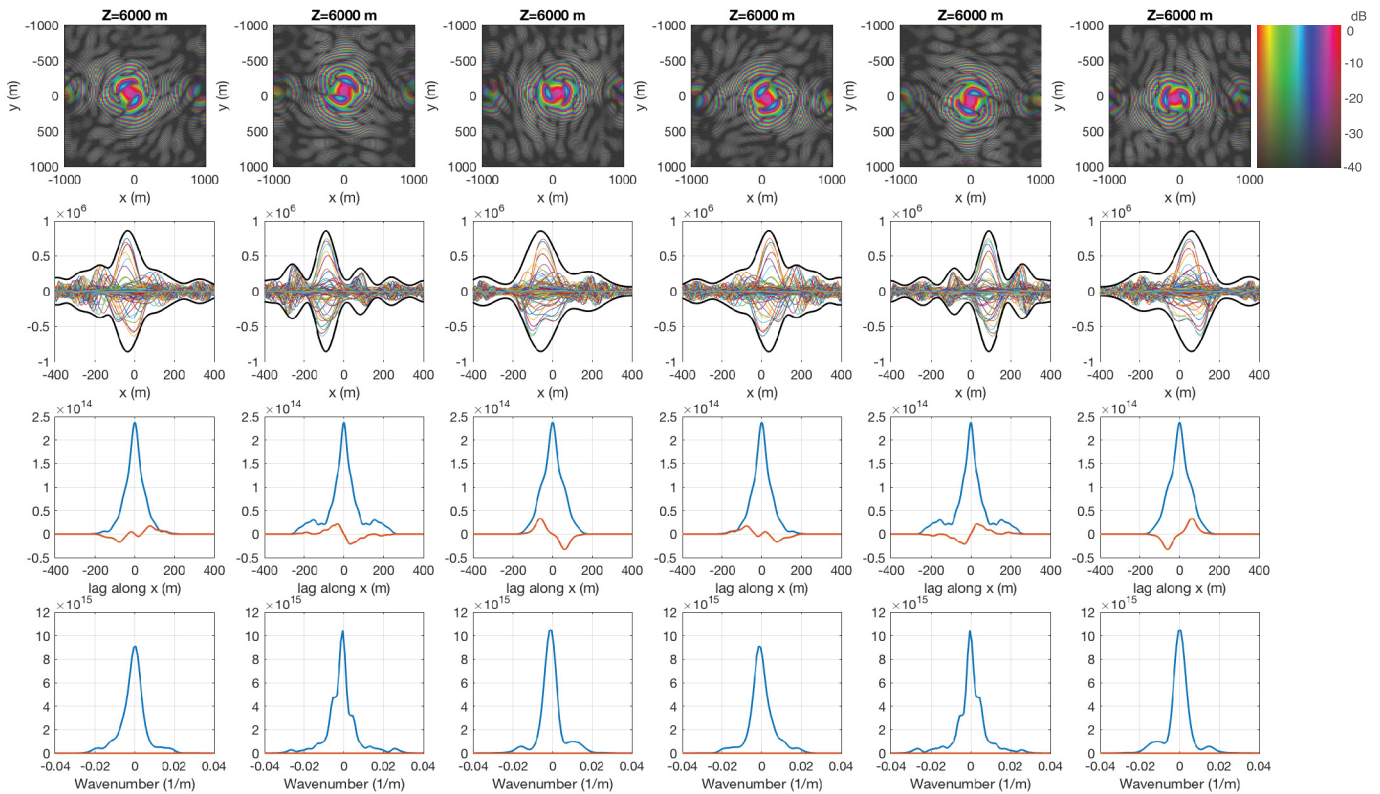
Fig. 5. Complex beam patterns (horizontal section), $G(\tau)$ and $\mathcal{F}[G(\tau)]$, at height $z = 6000$ m, calculated with respect to PANSY radar, are plotted. Columns 1–6 are associated with an azimuthal rotation angle of $0°$, $60°$, $120°$, . . . , $300°$, respectively. Rows: (a) Complex beam patterns (horizontal section) plotted with a 2-D color code indicating phase by hue (cyclic color) and power in dB by intensity. When the rotation angle is $0°$, the x-axis agrees with the physical x-axis. (b) Sections of the complex beam patterns plotted in row (a). Thin colored lines show the x-sections at different y intercepts. Thick black lines show their RMS envelopes. (c) Sum of ACFs of the sections of the complex beam pattern, $G(\tau)$ in the text, but plotted as functions of the distance in meter unit along the x-axis. Blue and red lines indicate the real and imaginary parts, respectively. (d) Fourier transforms of the $G(\tau)$ shown in Row (c), $\mathcal{F}[G(\tau)]$ are plotted as functions of wavenumber (1/m). The wavenumber can be converted to velocity simply by multiplying $|\boldsymbol{u}|$.

VI. DISCUSSION

We chose the PANSY radar as an instance to which the proposed beam debroadening technique was applied because the radar has an uneven and asymmetric antenna arrangement, and consequently a complicated beam pattern that makes it hard to evaluate the beam broadening effect. As the PANSY radar has quite a large aperture of about $450\lambda^2$, however, the resulting broadening effect was rather small although detailed quantitative discussions about the absolute significance of the broadening effect in relation with aperture size and antenna arrangement are out of the scope of this article. Note that, however in general, a radar with smaller aperture has a larger broadening effect. A recent study by Kohma *et al.* [15] showed that the turbulent spectrum variance as small as 100 mm/s has a significant meaning in discussing the energy dissipation rate. In addition, in the context of global circulation, a subtle background velocity as small as 10 mm/s can be significant. In such cases, our proposed method plays a more significant role.

Furthermore, we would like to discuss the practical spectral width and frequency resolution. With large aperture VHF atmospheric radars, the typical time resolution is about 1 min. Using the Blackman–Tukey method, for example, the frequency resolution can be consequently as small as 1/60 Hz, which corresponds to 0.05 m/s at a radar frequency of 47 MHz. From the point of view of historically accumulated data, to which the Bartlett or a similar method had been applied due to the limitation in computational cost, the time resolution had been about several to 10 s, which corresponds to around 0.3 m/s. In this article, we showed that our proposed method works well even in such a case that the frequency resolution in data is not well defined. In case one would like to begin an observation accompanied by our proposed analysis technique, it is recommended to define a higher frequency resolution.

We would also like to place some technical notes with respect to the implementation of the proposed algorithm. Calculating $G(\tau)$ as a function of $\boldsymbol{u} = (u, v, w)$, which is a 3-D parameter, as well as beam direction and height, is slightly computationally heavy. In a practical implementation, $G(\tau)$ can be well approximated by first calculating $G_{\text{hor}}(\xi)$ corresponding only to the azimuth direction of the wind $\phi = \tan^{-1}(v/u)$, second stretching it to obtain $G_{\text{hor}}(\tau)$ in accordance with the horizontal wind velocity (u, v), and finally applying uniform phase rotation correspondingly to w to obtain $G(\tau)$. Thus, we can reduce the total computation cost by preparing a practical set of $G_{\text{hor}}(\xi)$ corresponding to a set of discrete azimuth direction, namely $\{G_{\text{hor}}(\xi; \phi_i) | \phi_i = 0, 1, \ldots, 359 \text{ in degrees}\}$, for example.
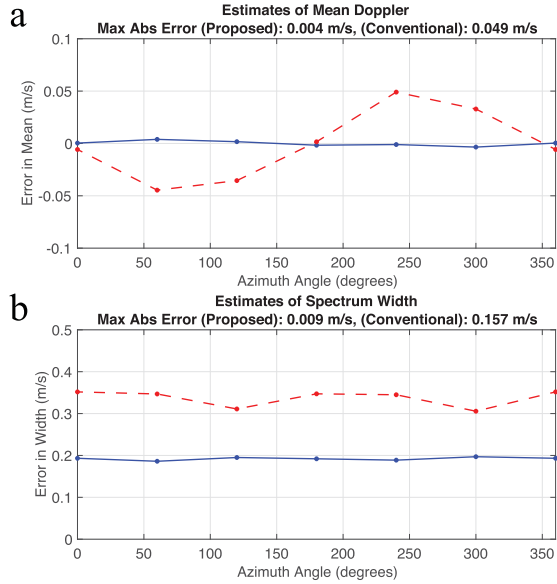
Fig. 6.   Estimates of (a) mean Doppler shift μ and (b) spectral width σ resulting from the simulations. In each panel, the red dashed and blue solid curves denote the conventional LMS estimates (without debroadening) and our proposed debroadening algorithm, respectively.

VII. CONCLUSION

We proposed a debroadening algorithm that estimates the turbulence spectrum width from the observed spectral width. By carefully examining the radar observation model from a statistical point of view, we derived the elegant relationship between the observation function (complex two-way radar beam pattern), statistical properties of the turbulence, and the length of the temporal window in the domain of the ACF shown in (31). Based on the derived relationship, we constructed the debroadening algorithm using generic iterative numerical inversion techniques. Although the algorithm was intended for debroadening the width of observed spectra, our numerical simulation showed that the algorithm also resolves biases in the mean Doppler shift that arises when the array is not symmetric. In this article, we employed a four-parameter model as the turbulence spectrum. However, the technique is not restricted to this model and can be enhanced to a nonparametric method when sufficient data are provided. Our proposed technique is already used in recent work [15].

APPENDIX A
DERIVATION OF BARTLETT PERIODOGRAM VIA ACFS

We briefly show the equality of the averaged periodograms (the Bartlett method) and the Fourier transform of ACFs similar to the Blackman–Tukey method.

Bartlett Spectrum via ACF

Let $R_\zeta[\nu]$ be the ACF of the ζth segment of a received signal $r_\zeta[n]$. That is

$$R_\zeta[\nu] = \begin{cases} \sum_{n=0}^{N-\nu-1} r_\zeta^*[n]\, r_\zeta[n+\nu], & \text{for } \nu \geq 0 \\ \sum_{n=-\nu}^{N-1} r_\zeta^*[n]\, r_\zeta[n+\nu], & \text{for } \nu < 0. \end{cases} \tag{39}$$

The DFT of $R_\zeta[\nu]$ becomes

$$\mathcal{R}[\kappa] = \sum_\zeta \sum_{\nu=1-N}^{N-1} R_\zeta[\nu]\, \exp\left(j2\pi \frac{\nu\kappa}{N} \right) \tag{40}$$

$$= \sum_\zeta \sum_{\nu=0}^{N-1} \left(R_\zeta[\nu] + R_\zeta[\nu - N] \right) \exp\left(j2\pi \frac{\nu\kappa}{N} \right) \tag{41}$$

where the second equation is obtained because

$$\exp\left[j2\pi \frac{(\nu \pm N)\kappa}{N} \right] = \exp\left(j2\pi \frac{\nu\kappa}{N} \right) \quad \forall\nu. \tag{42}$$

Note that the divisor in the exponential function of the "DFT" is N, and it does not agree with the length of the nonzero part of $R_\zeta[\nu]$, which is $2N - 1$. This is because the independent degrees of freedom of $R_\zeta[\nu]$ are N, and this does not cause any loss of information. If one applies the ordinary $2N$-point DFT to $R_\zeta[\nu]$, $-N \leq \nu \leq N - 1$, where $R_\zeta[-N] = 0$, the points $\mathcal{R}[\kappa]$ for $\kappa = $ odd in the resulting spectrum can be calculated from the rest of the points $\mathcal{R}[\kappa]$ for $\kappa = $ even just by interpolating.

Bartlett Method

$$3\mathcal{R}[\kappa] = \sum_\zeta \left| \sum_{n=0}^{N-1} r_\zeta[n]\, \exp\left(j2\pi \frac{n\kappa}{N} \right) \right|^2 \tag{43}$$

$$= \sum_\zeta \left\{ \sum_{n=0}^{N-1} r_\zeta[n]\, \exp\left(j2\pi \frac{n\kappa}{N} \right) \right\}^*$$

$$\times \left\{ \sum_{n'=0}^{N-1} r_\zeta[n']\, \exp\left(j2\pi \frac{n'\kappa}{N} \right) \right\} \tag{44}$$

$$= \sum_\zeta \left\{ \sum_{n=0}^{N-1} \sum_{n'=0}^{N-1} r_\zeta^*[n]\, r_\zeta[n']\, \exp\left(j2\pi \frac{(n'-n)\kappa}{N} \right) \right\} \tag{45}$$

$$= \sum_\zeta \left\{ \sum_{n=0}^{N-1} \sum_{\nu=-n}^{N-n-1} r_\zeta^*[n]\, r_\zeta[n+\nu]\, \exp\left(j2\pi \frac{\nu\kappa}{N} \right) \right\} \tag{46}$$

and by exchanging the order of summation with respect to n and ν in (46), we obtain (41).

APPENDIX B
FOURIER TRANSFORM OF GAUSSIAN FUNCTIONS

Let ν and κ be integer temporal and frequency variables, respectively, ranging from $[-N/2, N/2 - 1]$ for even N. The four-parameter Gaussian spectral model can be defined as

$$\mathcal{R}[\kappa] = A \exp\left[-\frac{(\kappa - \mu)^2}{2\sigma^2} \right] + P_n \tag{47}$$

where A, σ, μ, and P_n are the amplitude, spectral width, spectral moment, and noise level, respectively. Then, the corresponding ACF becomes

$$F[\nu] = A \frac{\sqrt{2\pi}\,\sigma}{N} \exp\left[-\frac{2\pi^2\sigma^2\nu^2}{N^2} + j\frac{2\pi\nu\mu}{N} \right] + P_n\,\delta[\nu] \tag{48}$$

where $\delta[\nu]$ is the discrete delta function, which is $\delta[0] = 1$, and $\delta[\nu] = 0 \ \forall \ \nu \neq 0$. These two functions form a DFT pair

$$\mathcal{R}[\kappa] \Leftrightarrow F[\nu]. \tag{49}$$

Unlike cases with an (analytic) Fourier transform, however, this expression can hold only when the parameters are set within a fair range because this expression is a simple analog of a Fourier transform, in which the sampling theory and the variable ranges are not considered. A practical fair range is, for example

$$-\frac{N}{2} \lesssim \mu \pm 3\,\sigma \lesssim \frac{N}{2}. \tag{50}$$

ACKNOWLEDGMENT

REFERENCES

[1] W. K. Hocking, "Measurement of turbulent energy dissipation rates in the middle atmosphere by radar techniques: A review," *Radio Sci.*, vol. 20, no. 6, pp. 1403–1422, Nov. 1985.

[2] W. K. Hocking, "On the extraction of atmospheric turbulence parameters from radar backscatter Doppler spectra—I. Theory," *J. Atmos. Terr. Phys.*, vol. 45, nos. 2–3, pp. 89–102, Feb. 1983.

[3] W. K. Hocking, "Observation and measurement of turbulence m the middle atmosphere with a VHF radar," *J. Atmos. Terr. Phys.*, vol. 48, no. 7, pp. 655–670, Jul. 1986.

[4] W. K. Hocking, "The dynamical parameters of turbulence theory as they apply to middle atmosphere studies," *Earth, Planets Space*, vol. 51, nos. 7–8, pp. 525–541, Jul. 1999.

[5] S. Sommer and J. L. Chau, "Patches of polar mesospheric summer echoes characterized from radar imaging observations with MAARSY," *Annales Geophysicae*, vol. 34, no. 12, pp. 1231–1241, Dec. 2016, doi: 10.5194/angeo-34-1231-2016.

[6] T. Sato and R. F. Woodman, "Spectral parameter estimation of CAT radar echoes in the presence of fading clutter," *Radio Sci.*, vol. 17, no. 4, pp. 817–826, Jul. 1982, doi: 10.1029/RS017i004p00817.

[7] R. F. Woodman, "A general statistical instrument theory of atmospheric and ionospheric radars," *J. Geophys. Res.*, vol. 96, no. A5, pp. 7911–7928, 1991, doi: 10.1029/90JA02628.

[8] E. Kudeki, S. Bhattacharyya, and R. F. Woodman, "A new approach in incoherent scatter F-region $E \times B$ drift measurements at Jicamarca," *J. Geophys. Res.*, vol. 104, no. A12, pp. 28145–28165, 1999, doi: 10.1029/1998JA900110.

[9] J. L. Chau and E. Kudeki, "First E-and D-region incoherent scatter spectra observed over Jicamarca," *Annales Geophysicae*, vol. 24, no. 5, pp. 1295–1303, Jul. 2006, doi: 10.5194/angeo-24-1295-2006.

[10] T. E. VanZandt, "A dual-beamwidth radar method for measuring atmospheric turbulent kinetic energy," *Geophys. Res. Lett.*, vol. 29, no. 12, p. 1572, 2002, doi: 10.1029/2001GL014283.

[11] K. Sato *et al.*, "Program of the antarctic syowa MST/IS radar (PANSY)," *J. Atmos. Solar-Terr. Phys.*, vol. 118, pp. 2–15, Oct. 2014.

[12] W. K. Hocking, J. Röttger, R. D. Palmer, T. Sato, and P. B. Chilson, *Atmospheric Radar: Application and Science of MST Radars in the Earth's Mesosphere, Stratosphere, Troposphere, and Weakly Ionized Regions*. Cambridge, U.K.: Cambridge Univ. Press, 2016.

[13] M. Yamamoto, T. Sato, P. T. May, T. Tsuda, S. Fukao, and S. Kato, "Estimation error of spectral parameters of mesosphere-stratosphere-troposphere radars obtained by least squares fitting method and its lower bound," *Radio Sci.*, vol. 23, no. 6, pp. 1013–1021, Nov. 1988.

[14] J. Rice, "On the estimation of the parameters of a power spectrum," *J. Multivariate Anal.*, vol. 9, no. 3, pp. 378–392, Sep. 1979.

[15] M. Kohma, K. Sato, Y. Tomikawa, K. Nishimura, and T. Sato, "Estimate of turbulent energy dissipation rate from the VHF radar and radiosonde observation in the Antarctic," *J. Geophys. Res., Atmos.*, vol. 124, no. 6, pp. 2976–2993, 2019, doi: 10.1029/2018JD029521.

Koji Nishimura received the B.E. degree from Ritsumeikan University, Kyoto, Japan, in 1999, and the M.I. and Ph.D. degrees from Kyoto University, Kyoto, Japan, in 2001 and 2006, respectively.

From 2001 to 2003, he worked for Sony Corporation, Tokyo, Japan. Since 2007, he has been with the National Institute of Polar Research, Tokyo, where he is currently a Project Associate Professor. His major research interests include radar signal processing, multichannel signal processing, remote sensing for the atmosphere, and satellite communications.

Dr. Nishimura received the Prize for Science and Technology (in The Commendation for Science and Technology by the Minister of Education, Culture, Sports, Science and Technology) from the Japanese Government in 2014.

Masashi Kohma received the B.S. degree from Kyoto University, Kyoto, Japan, in 2009, and the M.S. and Ph.D. degrees from The University of Tokyo, Tokyo, Japan, in 2011 and 2014, respectively.

He stayed at Syowa Station, Antarctic, as a wintering party member from 2015 to 2017. He is currently an Assistant Professor with the Department of Earth and Planetary Science, The University of Tokyo. His research interests include middle atmosphere dynamics, tropopause, polar stratospheric/mesospheric clouds, and estimation of turbulent parameters in the atmosphere.

Kaoru Sato received the B.S. and M.S. degrees from The University of Tokyo, Tokyo, Japan, in 1984 and 1986, respectively, and the Ph.D. degree from Kyoto University, Kyoto, Japan, in 1991.

She worked as an Assistant Professor with The University of Tokyo and Kyoto University and as an Associate Professor with the National Institute of Polar Research. She also stayed at Syowa Station, Antarctic, as a wintering party member from 2002 to 2004 and a summer party member from 2018 to 2019. She is a Professor of atmospheric physics with The University of Tokyo. She is also the Leader of the Program of the Antarctic Syowa (PANSY) mesosphere-stratosphere-troposphere/incoherent scatter radar. She has contributed to studies of the dynamics of atmospheric gravity waves in terms of their generation, propagation, and interaction with the mean flow. Her research interest includes interhemispheric coupling processes that arise through the interplay of Rossby waves and gravity waves in the middle atmosphere. She has tackled this topic using a combination of high-resolution observations and numerical model simulations.

Dr. Sato was a recipient of the Commendation for Contributors to Promotion of an Oceanic State from the Prime Minister of Japan and the Prize for Science and Technology from the Minister of Education, Culture, Sports, Science and Technology of Japan.

Toru Sato received the B.E., M.E., and Ph.D. degrees in electrical engineering from Kyoto University, Kyoto, Japan in 1976, 1978, and 1982, respectively.

He has been with Kyoto University since 1983, where he is the Vice Director and a Professor with the Institute for Liberal Arts and Sciences, Kyoto. His major research interests include system design and signal processing aspects of atmospheric radars, radar remote sensing of the atmosphere, observations of precipitation using radar and satellite signals, radar observation of space debris, and imaging with ultra-wideband (UWB) pulse radars.

Dr. Sato is a fellow of the Institute of Electronics, Information, and Communication Engineers of Japan, and a member of the Society of Geomagnetism and Earth, Planetary and Space Sciences, and the Institute of Electrical and Electronics Engineers.